Solid State Ionics 6 (1982) 65–77
North-Holland Publishing Company

ANALYSIS OF HYDROGEN-DOPED LITHIUM NITRIDE ADMITTANCE DATA

J. Ross MACDONALD
Department of Physics and Astronomy, University of North Carolina, Chapel Hill, NC 27514, USA

A. HOOPER
Materials Development Division, AERE Harwell, Oxford, UK

and

A.P. LEHNEN
Department of Physics and Astronomy, University of North Carolina, Chapel Hill, NC 27514, USA

Received 8 May 1981

Admittance data taken at seven temperatures from ≈24 to 182°C on a hydrogen-doped lithium nitride single crystal with gold electrodes perpendicular to the *c* axis are analyzed using non-linear complex least-squares fitting, and the results are presented as three-dimensional perspective plots. An equivalent circuit used in previous fitting is shown to be inadequate and an improved one, which requires an inductance to yield good results at high frequencies and temperatures, is proposed and used. This circuit is partly based on previous small-signal analysis and thus many of its parameter values, estimated from the complex least-squares fitting, may be interpreted in terms of more basic properties of the electrode/material/electrode system. The activation enthalpy for conduction is found to be ≈0.223 eV. In addition, an interface capacitance as well as a diffuse double layer capacitance are identified. The material appears to show both an electrode reaction and heterogeneous adsorption, and the dominant mobile carriers in either the interface layer or possibly in the entire material are tentatively identified as electrons. The very high calculated mobility of the charge carriers decreases exponentially with increasing temperatures.

1. Introduction

There has been considerable interest in lithium nitride as a candidate for solid electrolyte applications because of its high ionic conductivity. Work has been carried out on both polycrystalline [1,2] and single crystal [3,4] forms of the material, and it has been found [4,5] that when hydrogen is present in the material (possibly as NH^{2-}) the room-temperature conductivity increases very appreciably. Further, for single crystal material the conductivity is several orders of magnitude higher when measured perpendicular to the *c* axis than parallel to it, with or without hydrogen.

Since the work of one of the present authors [4] on this material, powerful non-linear complex least-squares fitting [6,7] and three-dimensional perspective plotting [7,8] techniques have become available. It was therefore felt worthwhile to demonstrate the power and applicability of these methods by applying them to some of the same admittance data previously analyzed by less sophisticated methods [4] with the hope that some additional physical insight into the behavior of this material might be generated. Note that the non-linear complex least-squares (NCLS) method which we employ allows both the real and imaginary parts of impedance or admittance data to be fitted simultaneously to a model (e.g. an equivalent circuit), yielding the statistically most reasonable estimates for the set of unknown parameters (and

their uncertainties) which appear in the model. In addition, the weighting to be used in the least-squares fitting is freely selectable.

2. Preliminary analysis

The specimen selected for re-analysis was crystal L20, hydrogen doped, fitted with evaporated gold electrodes, and having an electrode area $a = 0.23$ cm^2 and an electrode separation $l = 0.08$ cm [4]. Only admittance data obtained for measurements perpendicular to the c axis were considered. Although the original measurements spanned the range from 1 Hz to 1 MHz, it was found that data in the range from 300 kHz to 1 MHz usually contributed little to helping determine the best equivalent circuit and parameter estimates. Thus, whenever a better fit could be obtained by using data extending only to 278 kHz rather than that obtained using all the data, the former fit was accepted. In the following, admittance data are analyzed for seven temperatures extending from 23.5 to 182°C.

Fitting to two different equivalent circuits was investigated: the ladder circuit designated "A" and the circuit designated "B" in fig. 1; the B circuit was used in the earlier analysis of these data [4]. The capacitance C_g in B was previously associated with the geometrical capacitance of the specimen. Since the dielectric constant of Li_3N appears [9] to be $\approx$10.5, one can calculate that for specimen L20 the geometrical capacitance, C_g, should be $\approx$2.7 pF. Now it is found that the high-frequency limiting resistance, R_∞, of L20 at room temperature (where it is greatest for the present temperature range) is $\approx$133 Ω. It then follows that if we define a frequency f_∞ from $\omega_\infty R_\infty C_g = 1$, we find that $f_\infty \approx 443$ MHz at room temperature. In order to be able to determine this C_g from ac measurements, such measurements would thus have to extend to 50 MHz or higher, much higher than the present measured limit. Therefore, the present measurements should be unable to yield an estimate of C_g, and any value actually obtained for it from equivalent circuit fitting should not be so identified with the geometric capacitance. Capacitative terms associated with the leads and instrumentation may contribute to any observed value of C_g. Note that we expect $R_\infty = R_1 \approx R_B$ in circuits A and B.

3. Equivalent circuits

The usefulness of two different equivalent circuits in representing the L20 data is investigated herein. One of these, circuit B of fig. 1, was picked because it was used in the earlier work [4]. Fitting of the data to this circuit to yield parameter estimates was carried out there by complex-plane techniques, however, rather than by the more objective and powerful NCLS approach used here. In circuit B, $R_B \equiv R_\infty$, the bulk resistance, and R_{IF} and C_{IF}, which were intensive rather than extensive quantities, were interpreted as being associated with a $\approx$200 Å thick interface layer of $LiOH/Li_2CO_3$ at the electrodes. Although no values for C_{IF} were quoted in ref. [4], a plane-parallel capacitor of this thickness and the L20 area would have a capacitance of $\approx$107 nF, using $\epsilon = 10.5$. Both R_B and R_{IF} were found to be thermally activated with activation enthalpies, ΔH, of $\approx$0.23 and 0.6 eV, respectively.

The A circuit of fig. 1 was picked both because it gave a much better fit than did B and also because a

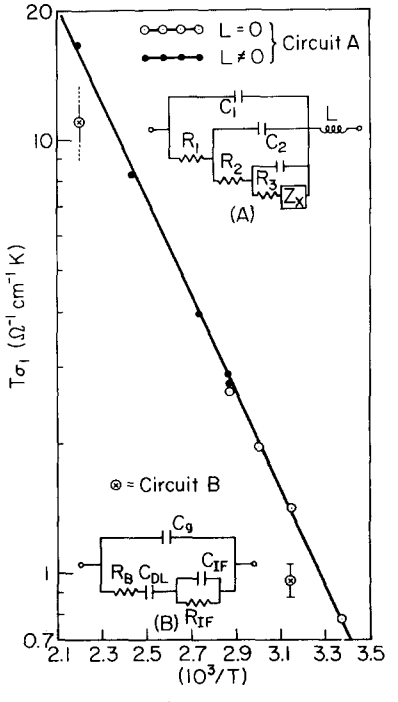

Fig. 1. Arrhenius plot of bulk conductivity times temperature versus $10^3/T$. The two equivalent circuits used for complex least-squares fitting are also shown.

circuit of this type with $L = 0$ follows from a detailed microscopic theory of charge motion in a material with charge of only a single sign mobile [10,11]. The impedance Z_x is zero if charges of opposite sign are completely immobile [11] but is a finite-length Warburg impedance [10,11], Z_w, when reaction products can diffuse in the electrode region [12]. We tried fitting the data with various choices for Z_x and found that a constant-phase-element (CPE) impedance (associated with a distributed process) led to far better results over the entire temperature range than the choices $Z_x = 0$ or even $Z_x = Z_w$. The addition of the inductance L to the circuit is discussed later.

The CPE admittance used by Huggins and coworkers (e.g. ref. [13]) is of the form

$$Y_x \equiv Z_x^{-1} = A_0\omega^\alpha + iB_0\omega^\alpha, \quad (1)$$

where $0 < \alpha < 1$ and A_0 and B_0 are frequency-independent parameters. It was soon pointed out [14,15], however, that the Kronig–Kramers relations (associated with causality) require that $B_0/A_0 = \tan(\alpha\pi/2)$, and thus that these parameters are not independent. Nevertheless, Huggins and his group still seem to determine them as separate constants in their curve fitting [2,15], an inappropriate approach in our opinion involving, as it does, an unwarranted degree of freedom. When the above relation between A and B is incorporated, the CPE Y_x reduces to

$$Y_x = A(i\omega)^\alpha, \quad (2)$$

where A is a new frequency-independent constant. Instead of three constants to determine, there are now only two, and the Y_x of eq. (2) satisfies the Kramers–Kronig relations as it must. Thus, for the Z_x of circuit A we have employed $Z_x = Y_x^{-1}$, using the Y_x of eq. (2). This form has in recent years been shown by Jonscher [16] to fit a great deal of data, although a complete microscopic theory leading to such a Z_x is still lacking.

It is of interest to note that an expression in complete agreement with that of eq. (2) was suggested as a network function of interest for solids (frequency and transient response) as early as 1956, and that the above B_0/A_0 relation appears there [17]. Since the distribution of relaxation times associated with an expression of this type is not normalizable, it strictly does not represent a physically realizable function [17], but a simple change in the form of Z_x as $\omega \to \infty$ cures this ailment [8] and need not be considered here since the frequency span of present interest is limited.

It should be emphasized that circuit A is not proposed as the best or necessarily most appropriate circuit to represent these data. Picking the best out of an infinity of possibilities is often impossible. Although a circuit with a different structure than that of A or one with even more free-parameter circuit elements might very well yield better fits, circuit A is sufficient for a preliminary analysis and interpretation, and its shortcomings may suggest useful modifications.

4. Fitting results

Table 1 presents some NCLS fitting results for L20 data and circuits A and B. Although some fitting with unity weighting (ordinary "unweighted" least squares) was carried out, it was always found that weighting derived on the basis that all individual real and imaginary data values had uncertainties proportional to their magnitudes (P weighting) gave far superior results, and the latter weighting was used for all the fits in table 1. The notation $Q|\gamma$ used in table 1 indicates the estimated values obtained from NCLS fitting of a parameter Q and its relative uncertainty γ (relative standard deviation). All fitting was carried out for data in admittance form. For the full A circuit, parameter estimates obtained from fitting corresponding impedance data were generally within one of their standard deviations of corresponding admittance estimates but this was very much not the case for the other fits. All resistances are here given in Ω, capacitances in nF, and inductances in μH. No C_1 values are presented for the A-circuit fits because fitting runs with C_1 free always led to $C_1 \approx 0$ and completely uncertain. For the frequency range covered, C_1 values could thus not be adequately determined from the data, in agreement with the results of the preliminary analysis when C_1 is identified with C_g, the actual geometrical capacitance. Finally, the row 9 A-circuit results are the only ones here where the data fitted extended to 1 MHz.

In table 1, σ_f is the estimated standard deviation of the entire fit. It was always found to be three or

Table 1
Estimated parameter values and their estimated relative standard deviations obtained from complex least squares fitting using circuits A and B for various temperatures. The quantity σ_f is the standard deviation of the overall fit

T (°C)	No. CKT	σ_f	A: R_1 B: R_B	A: R_2 B: R_{IF}	A: C_2 B: C_{IF}	A: R_3 B: C_g	A: C_3 B: C_{DL}	A: 10^6A	A: α	A: L
23.5	1-A	0.190	127.5|0.038	0	19.09|0.11	0	0	6.591|0.054	0.4978|0.018	0
	2-A	0.174	136.4|0.034	1687|0.10	37.86|0.046	0	0	5.662|0.058	0.5778|0.025	0
	3-A	0.103	133.0|0.020	978.8|0.074	32.42|0.034	3481|0.058	64.50|0.072	4.542|0.039	0.6901|0.017	0
45.0	4-A	0.169	83.04|0.033	658.0|0.050	55.35|0.046	0	0	5.268|0.039	0.7665|0.012	0
	5-A	0.070	78.66|0.014	272.8|0.050	40.68|0.028	754.4|0.036	118.9|0.057	4.894|0.017	0.7967|0.006	0
	6-B	0.375	115.8|0.090	1323|0.090	87.6|0.10	1.8|0.24	2471|0.068	–	–	–
59.4	7-A	0.052	58.97|0.010	137.0|0.037	54.64|0.023	292.6|0.033	193.7|0.053	5.797|0.012	0.8117|0.003	0
75.7	8-A	0.072	46.37|0.012	82.10|0.061	94.53|0.033	139.0|0.070	308.5|0.11	6.946|0.017	0.8023|0.005	0
	9-A	0.078	41.96|0.011	53.69|0.059	61.10|0.033	138.0|0.049	198.8|0.075	7.110|0.017	0.8052|0.005	2.88|0.032
	10-A	0.069	44.24|0.018	69.31|0.068	80.12|0.056	137.6|0.055	252.0|0.092	7.022|0.016	0.8042|0.004	1.27|0.29
93.2	11-A	0.039	32.06|0.007	34.27|0.038	117.6|0.028	93.86|0.035	333.4|0.043	9.408|0.009	0.7850|0.003	3.04|0.024
138.0	12-A	0.033	17.34|0.005	14.64|0.060	592.1|0.023	65.06|0.090	773.1|0.048	10.46|0.009	0.7613|0.003	3.54|0.017
182.3	13-A	0.070	9.45|0.011	19.93|0.13	1394|0.032	0	0	13.60|0.015	0.7699|0.004	4.25|0.028
	14-A	0.067	9.46|0.010	33.68|0.089	1502|0.025	354.8|0.11	1496|0.045	11.71|0.020	0.7485|0.007	4.02|0.026
	15-B	0.644	14.3	3×10^{-7}	10.7	0	3636	–	–	–

more times larger for circuit B fits than for circuit A ones. Because of the presence of residual systematic errors (of the wrong-model type [18]) in most of these results, both the σ_f and parameter relative standard deviations are likely to be underestimates but should still be of value for comparisons.

Since the circuit B fits were invariably much worse than the A ones, we have presented only representative low- and high-temperature results for B (lines 6 and 15). Notice that for the 45.0°C B fit the estimate of C_g is very uncertain (and no such estimate could even be obtained for the high-temperature fit). Further, the C_g value found here is nearly 700 times larger than the expected geometrical capacitance. Thus this "C_g" cannot be an estimate of the actual geometrical term and is also too large to be explained in terms of experimental artifacts. A large value appears here only because the B circuit is a poor choice for these data. No estimated standard deviations are presented for high-temperature B fit because the fit was so poor that none could be calculated (and such estimates would be so large that they would be meaningless anyway). Although the B-fit results yield an activation enthalpy for $T\sigma_B$ in reasonable agreement with that obtained from A fits, the results in table 1 show that the magnitude of the bulk resistance, R_B, is considerably overestimated for B fits. Note that the B fits yield an essentially zero value for R_{IF} at $T = 182.3$°C and that C_{IF} appears to decrease with increasing temperature, contrary to normal expectation.

The fitting results indicate that all the circuit elements of the A circuit involve thermal activation. Activation enthalpy results and interpretation will be discussed in section 5. Some consideration of plausible temperature dependence for quantities like α has been given earlier [19], but lacking a microscopic theory of the present Z_x, the results for α cannot be further interpreted from a physical point of view.

The inductance L has been included in the A circuit because it was found essential in order that a good fit could be obtained at the higher temperatures. For $T < 75$°C, the data did not allow a non-zero estimate of L to be obtained, even with the full frequency range used. The magnitude of the reactance of a 3 μH inductance is $\approx$5 and 20 Ω at 278 and 1000 kHz, respectively. Only at the higher temperatures where the magnitude of the impedance of the rest of the circuit is comparably small, can L be well determined. The full frequency span was only used for the results of line 9 in table 1; all others used the restricted range. Comparison of the line 9 and 10 results show that a good estimate of L could not be obtained at this temperature with the restricted range but such estimates were found at the higher temperatures.

In spite of the small temperature dependence of the estimated L values (to be discussed later) it is reasonable to expect that L itself arose from wiring inductance in the measuring apparatus. To obtain an inductance of 3 μH would require an unrealistic length of $\approx$60 m of isolated straight wire but only a single circular loop of no. 18 wire of 36 cm radius, not an unlikely possibility. Had measurements been made with the same apparatus with a short circuit in place of the sample, the resulting impedance values could have been subtracted from those obtained with the sample in place, eliminating any series wiring effects. Since L is here absolutely necessary in order to get a good fit at the higher temperatures, the present analysis shows how complex least-squares analysis can identify and compensate for such residual effects when present.

The first three rows in table 1 have been included to show how the fit improves as R_2 and then R_2, R_3, and C_3 are allowed to be free parameters in the fitting and thus different from zero. Clearly the 3-A results are superior. Even more improvement occurs at 45°C when the R_3 and C_3 elements are made free (rows 4-A, 5-A).

The row 9-A result for L is much more precise than that of 10-A, and this L value is taken as the best estimate at this temperature. But since the σ_f is better for the 10-A fit (using data only to 278 kHz) than for the 9-A fit, we have used the rest of the 10-A results in subsequent analysis.

Next, note that σ_f decreases with increasing temperature until $T \approx 138$°C, then increases. Further, comparison of the 13-A and 14-A results shows that the presence of R_3 and C_3 as free parameters does not improve the overall fit much here. The reversal of the temperature dependence trend of R_2 and R_3 as the temperature increases from 138 to 182°C also suggests that the full A circuit may not be the best possible choice at 182°C, although these reversals may conceivably be meaningful and may indicate the

presence of a new process not significant at lower temperatures. Incidentally, circuit B with an added series inductance does improve the fit at high frequencies for the higher-temperature data, as might be expected, but the overall improvement is slight and the fit remains far worse than that using circuit A. For example, for the 182°C data, the resulting σ_f found is 0.598; a "C_g" estimate of ≈52 nF is obtained; the other parameters are not much changed; and the new L value is ≈9 μH. The fit is still inadequate to allow meaningful conclusions to be made.

The next four figures show what can be learned from three-dimensional perspective plots [7,8] of some of the present data. Since the larger magnitudes (which show up best on such plots) tend to appear at high frequencies for admittance data and at low ones for the corresponding impedance data, it is appropriate to include plots of both kinds. Fig. 2 presents such 3-D plots for the 45.0°C data and the results predicted using the B-circuit parameters (row 6-B of table 1). In all these plots the original data points, designated by solid squares, are connected by solid lines and the predicted data points are indicated by open triangles. All origins are at (0,0,0) unless otherwise stated. The projections to the [log(f), real] plane involve solid lines for the actual data points and dashed lines for the predicted points. The projections of the original or calculated data lines *in* the three planes use the same convention. Note that the back plane, either [Im(Y), Re(Y)] or [−Im(Z), Re(Z)], is the complex plane used in the past for admittance or impedance plane plots, respectively. As we see from figs. 2a and 2b, the inclusion of a log(f) axis allows one to apprehend at a glance far more details of the entire behavior of the three-dimensional response than does planar plotting.

Fig. 2a illustrates the very appreciable deviations between original and predicted B-circuit results, but fig. 2b shows that the low-frequency fit is even worse: A capacitor cannot do very well in simulating a CPE with $\alpha < 1$. Considerably better, but still somewhat imperfect, results are demonstrated in fig. 3, the A-circuit fit of the same data (row 5-A in table 1). Note that had conventional least-squares fitting of Re(Y) [or Im(Y)] versus f been carried out separately, the results would have been better but would have led to worse Im(Y) [or Re(Y)] results. Complex least-squares fitting achieves the best fit for Re(Y) and Im(Y) simultaneously. The fig. 3b results show that some accuracy in fitting the low-frequency

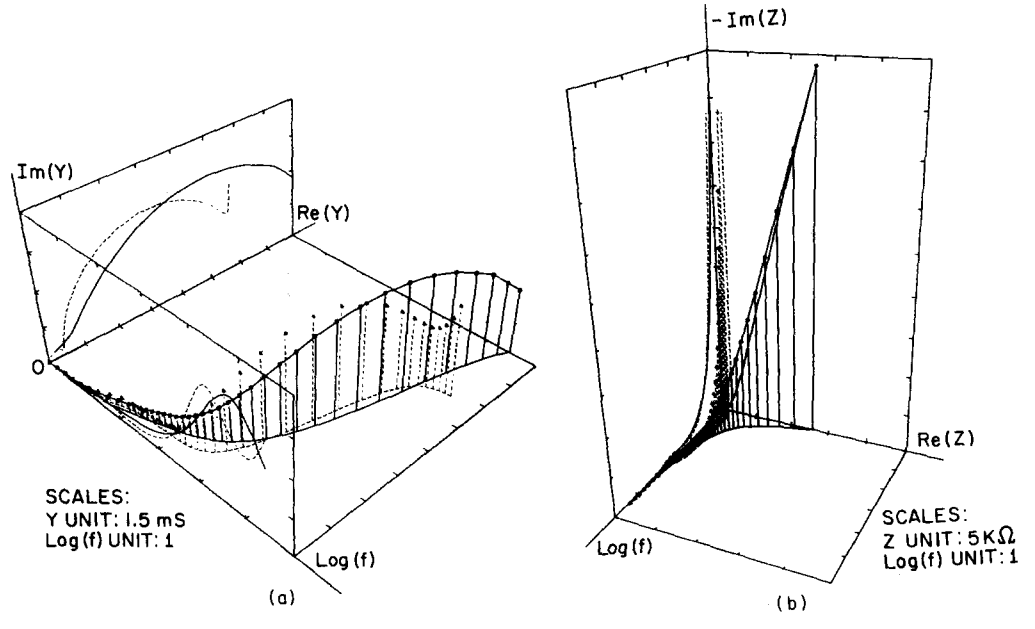

Fig. 2. Three-dimensional perspective plots of (a) admittance and (b) impedance for 45.0°C data (solid squares and solid lines) and circuit B fitting predictions (open triangles, dashed lines).

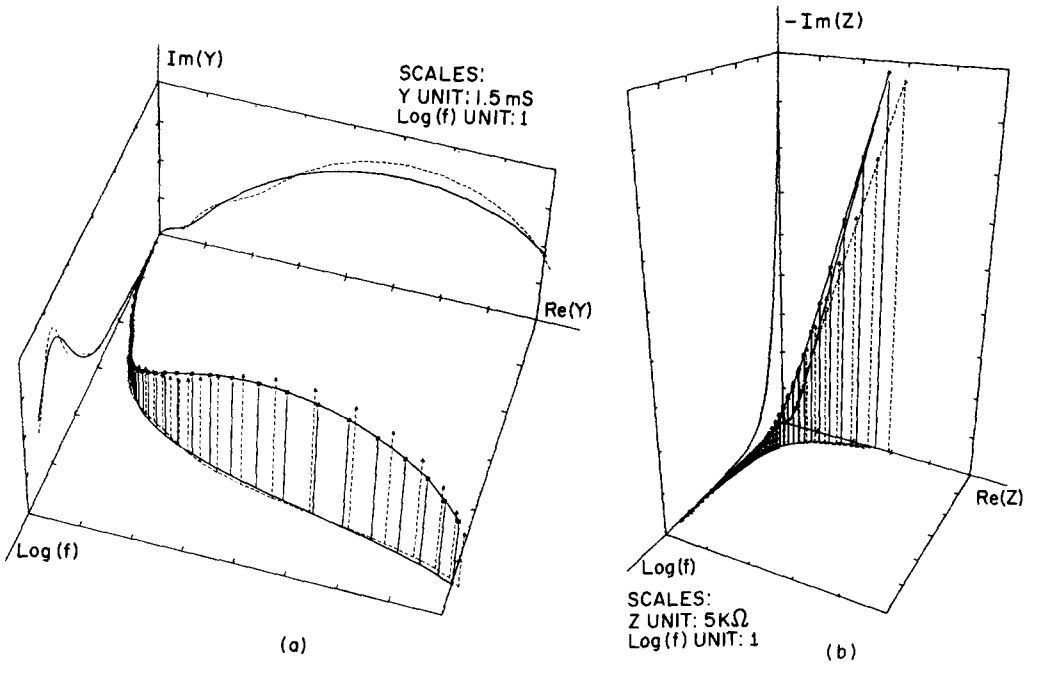

Fig. 3. Three-dimensional admittance and impedance plots for 45.0°C data and circuit A fitting predictions.

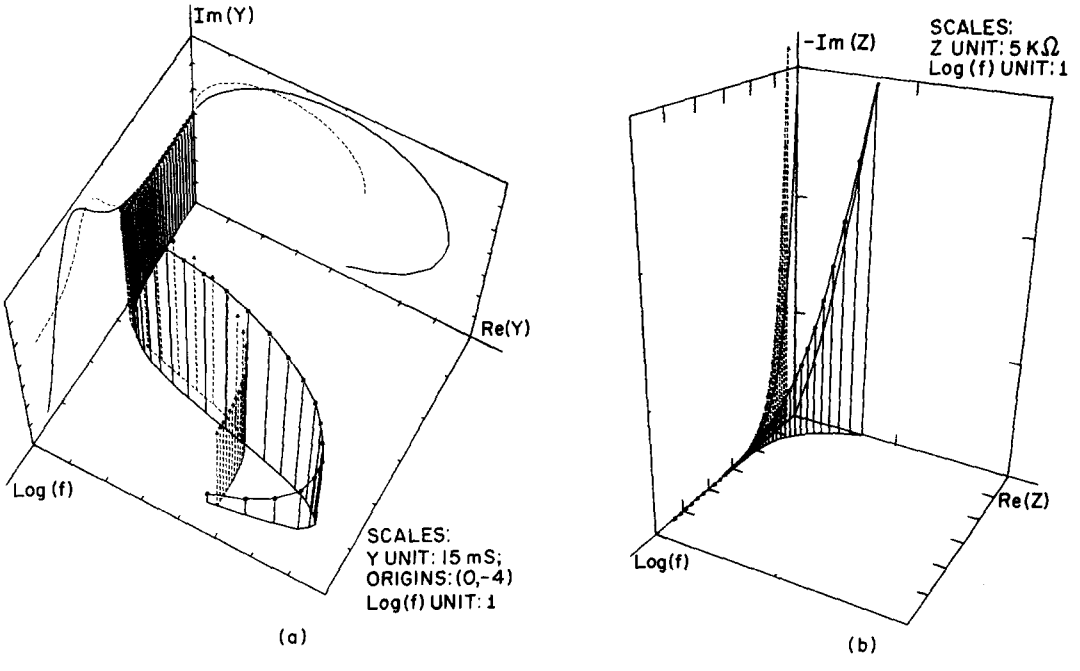

Fig. 4. Three-dimensional admittance and impedance plots for 182.3°C data and circuit B fitting predictions.

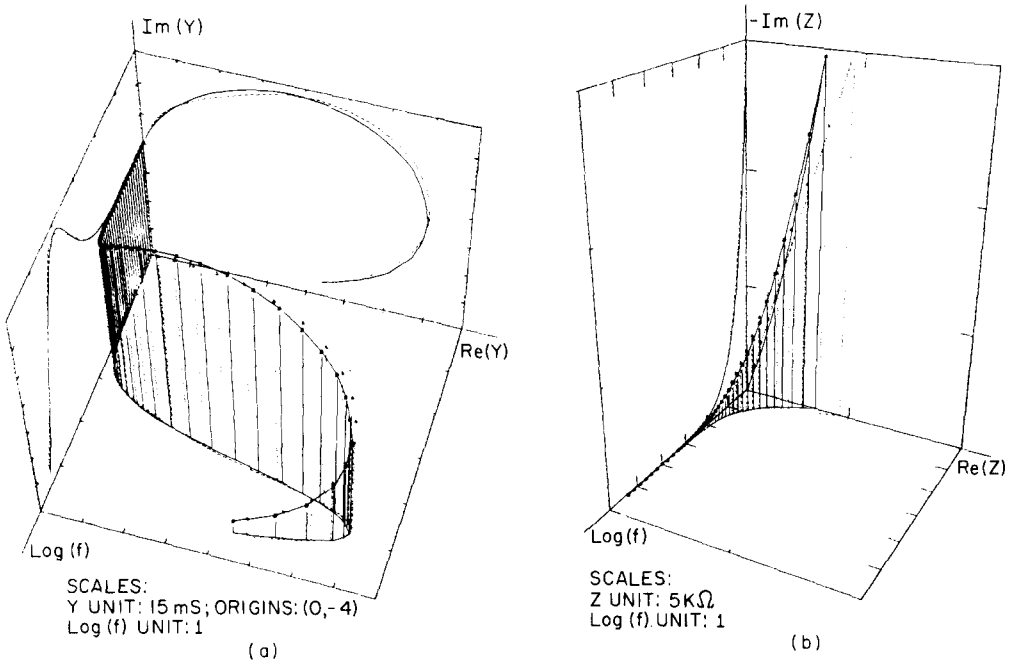

Fig. 5. Three-dimensional admittance and impedance plots for 182°C data and circuit A fitting predictions.

CPE slope in the impedance plane has been sacrificed to achieve better fits in the other two projected planes. It is thus clear that since the simple CPE does not allow a perfect fit it is not entirely appropriate for these data. Nevertheless, it is the best simple choice currently available.

Figs. 4 and 5 show 3-D results for $T = 182.3°C$ (rows 15-B, and 14-A in table 1). For clarity, the origin of the Im(Y) scale has been displaced downwards by four Y units (60 millisiemens) in figs. 4a and 5a. The true origin for the data is thus $+4Y$ units above the apparent one. This simple transformation has been made to allow the high-frequency negative admittance regions arising from L to show most simply.

Again we see in fig. 4 that the **B** circuit yields very poor fits, even allowing for the absence of an inductive term which, of course, precludes any negative admittances. It is clear, however, that given what it has to work with, the complex least-squares fitting has minimized the sum of squared deviations by predicting points which weave above and below (or around) the true points. Fig. 5 shows that the A-circuit allows quite good admittance fitting, but again the CPE falls quite short of perfection in the low-frequency region. Incidentially, when the Y data were converted to Z data and the latter fitted directly (Z fit), results were obtained which could not be easily distinguished from those shown. Thus, with P weighting and an adequate fitting circuit, it makes no practical difference for 3-D plots whether Y or Z fitting is carried out.

These results show that the A circuit is a good choice but is by no means an ideal one for these data. In addition to the inadequacy of the CPE, the 3a or 5a admittance plots show that though the predicted points often fall quite close in space to the true data line, they show some non-negligible deviations more or less along the line; that is, even if they are on the line, they may be at the wrong places on the line. In spite of these deficiencies, which only 3-D perspective plotting can show so clearly, we believe that the A circuit is adequate to allow meaningful analysis of its fitting results to be carried out. We have thus done so in the next section.

5. Analysis of results

The microscopic analysis of charge motion on which circuit A (without Z_x and L) is based leads to the identification $(R_1, C_1; R_2, C_2; R_3, C_3) = (R_\infty, C_g; R_R, C_R; R_A, C_A)$, where R_∞ and C_g are bulk (extensive) quantities and the "R" and "A" subscripts stand for "reaction" and "adsorption". Thus R_R is an intensive electrode reaction resistance and C_R is its associated capacitance, the diffuse double layer capacitance, C_{DL}. Fig. 1 has already demonstrated that $T\sigma_1 = T\sigma_\infty \approx T\sigma_B$ is thermally activated and fits the general form $Q = Q_0 \exp(-\Delta H_Q/kT)$ very accurately. Here Q is the thermally activated quantity and ΔH_Q is the associated activation enthalpy of the process. Fig. 6 (a semilog plot) shows that most of the other quantities derived from the fitting (or simple transformations of them) are also thermally activated.

Some discussion of the high-temperature deviations of the R_2 and R_3 results from simple activation behavior has already been given; there we see that the deviations associated with T/aR_2 and T/aR_3 are quite regular and that none occurs in TC_3/a. This suggests that the deviations may not, in fact, arise from fitting

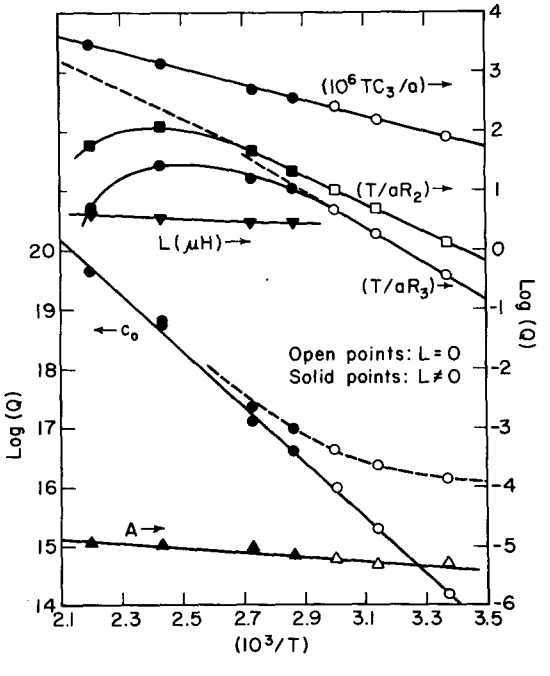

Fig. 6. Semilog versus $10^3/T$ plots for various quantities obtained from circuit A fitting results.

failures and an inappropriate circuit but may indeed indicate the onset of a new process at the higher temperatures. The units of C_3 in this plot are farads and those of L are microhenries.

The earlier work provides expressions relating measured circuit elements to more basic material and material/electrode processes. Using the above identifications, for charge of a single sign mobile one finds [10,11,20]

$$T\sigma_1 = Tl/aR_1 = Tec_0\mu = ec_0D/ke^{-1}, \tag{3}$$

$$C_2 = \epsilon a/8\pi L_D, \tag{4}$$

$$L_D = (\epsilon kT/4\pi e^2 c_0)^{1/2}, \tag{5}$$

$$k^* = (k_0 + i\omega\tau_a k_\infty)/(1 + i\omega\tau_a), \tag{6}$$

$$k_\infty = (k/e^2c_0)T/aR_2, \tag{7}$$

$$(k_0^{-1} - k_\infty^{-1})^{-1} = (k/e^2c_0)T/aR_3 \tag{8}$$

and

$$\tau_a = (k_0/k_\infty)R_3C_3 \equiv R_{23}C_3 = \frac{TC_3/a}{T/aR_2 + T/aR_3}. \tag{9}$$

In the last equation R_{23} is the parallel combination of R_2 and R_3. Since results are more complicated when charges of both signs are mobile and it is likely for the present situation that mobile charge of a single sign dominates the conductivity, we shall carry out a tentative interpretation of results on that basis. Notice, however, that we have not prejudged whether positive or negative mobile charge carriers dominate and have used neutral symbols such as D instead of D_n or D_p.

In eq. (4) 8π appears instead of 4π because there are two identical electrodes and C_2 is made up to the combination of two diffuse double layer capacitances in series, associated with an interphase region. The Debye length in eq. (5) applies for charge of a single sign mobile. In all this work we have assumed unity valence numbers for the positive and negative charges. The reaction/adsorption rate constants k_0 and k_∞ appear in the complex reaction rate expression [10] of eq. (6); they apply to the mobile, reacting carrier, and k_0 is the value of k^* at $\omega = 0$ and k_∞ that as $\omega \to \infty$.

More basic expressions for k_0, k_p, and the adsorption/reaction time constant τ_a appear written in terms of reaction rate derivatives in ref. [10] but are not needed here. Note that if TC_3/a, T/aR_2, and T/aR_3 are all thermally activated, it follows from eqs. (7)–(9) that k_0^{-1} and τ_a^{-1} may be expressed as the sum of two thermal activation formulas, $Q = Q_a + Q_b$, with different activation enthalpies.

Now if ϵ is taken temperature independent, eqs. (4) and (5) allow the bulk concentration c_0 to be calculated from $C_2(T)$ results. Results of this procedure are shown as the upper (dashed curve) set of c_0 points in fig. 6. Values of c_0 thus range from $\approx 4.5 \times 10^{19}$ cm^{-3} at $T = 182.3$°C down to $\approx 1.4 \times 10^{16}$ cm^{-3} at $T = 23.5$°C. But these results show that c_0 deviates from a straight line at temperatures below ≈90°C. This deviation is associated with the apparent approach of C_2 to a constant value as T decreases below this temperature. It is thus reasonable to replace eq. (4) by

$$C_2 = C_I + C_{DL} = (\epsilon a/4\pi)[(2l_I)^{-1} + (2L_D)^{-1}]. \quad (10)$$

Here C_I and l_I refer to a possible interface layer at the surface of the crystal (one at each end). In the earlier work [4], such a layer was identified and had an estimated thickness of ≈200 Å. Nuclear reaction analysis showed it to consist primarily of LiOH and Li_2CO_3. In our present fitting, we selected that value of C_I which led to the best thermal activation line for c_0, calculated from eq. (10). The value $C_I = 29$ nF gave the excellent (bottom-line) results shown for c_0 in fig. 6. If ϵ is, as usual, taken as 10.5, the resulting value of l_I is ≈ 370 Å. This is in relatively good agreement with the quoted experimental layer thickness, which was subject to considerable error. Note that the parallel connection of C_I and C_{DL} of eq. (10) implies that the diffuse layer charge can enter into the l_I region next to the electrode. At high temperatures, the large amount of space charge thus present in the interface layer might well modify C_I, making it a decreasing function of temperature. Although we have taken C_I temperature independent, a reduction of C_I with temperature at temperatures above 75°C would make little change in our results. Incidentally, the $T = 23.5$°C value of c_0 calculated with the $C_I = 29$ nF correction is $\approx 1.5 \times 10^{14}$ cm^{-3}, much smaller than that obtained without it.

Table 2
Least-squares fitting of quantities of the form $Q = Q_0 \exp[-\eta/T] = Q_0 \exp[-\Delta H/kT]$ or as the sum of two such exponentials

Quantity Q	Q_0	η (K)	ΔH_Q (eV)
$T\sigma_1$ (Ω^{-1} cm^{-1} K)	4622.56	2582.6	0.223
T/aR_2 (Ω^{-1} cm^{-2} K)	1.69272×10^8	5527.4	0.476
T/aR_3 (Ω^{-1} cm^{-2} K)	9.60399×10^9	7115.8	0.613
TC_3/a (F cm^{-2} K)	2.18033	3023.1	0.261
c_0 (cm^{-3})	1.01419×10^{30}	10788.6	0.930
A (Ω^{-1} Hz$^{-\alpha}$)	8.39988×10^{-5}	879.77	0.076
α	0.592838	−104.54	−0.009
L (μH)	12.0488	501.84	0.043
D (cm^2/s)	2.45145×10^{-12}	−8205.9	−0.707
k_∞ (cm/s)	8.97689×10^{-8}	−5261.2	−0.453
k_0^{-1} (s/cm)	1.96340×10^5 1.11397×10^7	3672.8 5261.2	0.317 0.453
τ_α^{-1} (s^{-1})	7.76362×10^7 4.40484×10^9	2504.3 4092.6	0.216 0.353

Table 2 summarizes the best-fit straight-line results of the fig. 1 and fig. 6 plots. The five lower-temperature points were used to obtain the T/aR_2 results and only the lower three were used for T/aR_3. Table 2 also includes results based on the six higher-temperature α values of table 1. The exponential fit given for α was found to be better than a linear fit with T^{-1}. However since the activation enthalpy is so small for α, it can almost be taken temperature independent above 25°C. Note that since ΔH_α is actually negative, it is α^{-1} which appears to be (slightly) thermally activated here.

There are a number of surprises in the results of table 2. The thermal activation of L, albeit with only $\Delta H_L \approx 0.04$ eV, is one of them. If L actually arises

from wiring inductance, the small temperature dependence found must be an artifact of the fitting, arising because the absolutely most appropriate circuit is not used, and probably induced through coupling to some of the other strongly temperature-dependent parameters of the circuit. Ionic inertial and scattering mechanisms have been invoked [21,22] to explain negative capacitance (or ordinary inductance) effects appearing in solid electrolyte impedance measurements at $\approx$1 MHz [21] and at $\gtrsim$ 1000 MHz [22]. However, the latter frequency range is far beyond that attained here, and there is also appreciable likelihood that the results of ref. [21] arose from residual effects rather than inertial ones [23]. Thus, we conclude that the present L is largely a property of the measuring apparatus and not of the material/electrode system itself.

The value of $\Delta H_{T\sigma_1}$ found here is close to the 0.23 eV found earlier [4] and is certainly more accurate. Further, although the final c_0 values obtained from the present analyses seem somewhat low, they are nevertheless of quite possible magnitudes. The ΔH_{c_0} value of $\approx$0.93 eV is reasonably close to the value of 0.83 eV found [24] by NMR and identified as the jump enthalpy of Li^+ ions in single crystal Li_3N. There seems to be some doubt about the validity of this result [24], and it should not equal ΔH_{c_0} in any case. It seems reasonable that the present c_0 results, derived as they are in a very straightforward way from well-determined C_2 fitting results, actually reflect to good accuracy the bulk concentration of dominant mobile charge in the crystal. Even if ϵ is temperature dependent, results would not be much altered. But the $T\sigma_1$ and c_0 results together allow one to calculate μ and D for the mobile charge carrier. They lead to D values of $\approx 2 \times 10^{-4}$ cm^2/s at 182.3°C and of 2.75 cm^2/s at 23.5°C. This latter value implies a mobility of $\approx$110 cm^2/V s! Now the largest $D = D_p$ we would expect for Li^+ ions would be 10^{-6}–10^{-5} cm^2/s. Although a value for the chemical diffusion coefficient of Ag^+ ions of 0.47 cm^2/s has been found from current decay measurements [25], it involves a large thermodynamic enhancement factor. But even if such a factor were operative in the present case, we see that D here *increases* with decreasing temperature rather than decreases in the usual way for thermally activated ionic motion in solids. It is strongly temperature dependent with a ΔH for D^{-1} of $\approx$0.71 eV. This result seems to completely preclude ionic conduction. In addition, the rate constants k_0 and k_∞ are also found to decrease with increasing temperature rather than to increase. This may be associated with a possible reduction of favored sites for reaction at the electrode with increasing temperature. The k_∞ and k_0 rate constants and the adsorption/reaction time constant, τ_a, calculated from the results in table 2, are $\approx$4 cm/s, 1 cm/s, and 5×10^{-5} s for 23.5°C and 10^{-2} cm/s, 5×10^{-3} cm/s, and 10^{-6} s for 182.3°C. respectively. Note that if $k_\infty = k_0$ there is no adsorption. With gold electrodes, it is difficult to see why any electrode reaction should be present if the reacting species were Li^+ ions, although there possibly might be a reaction involving oxygen present at the electrode interface.

All these difficulties are resolved if one gives up the idea that the dominant mobile charge carrier is Li^+. Boukamp and Huggins [26] found that treatment of Li_3N powder with hydrogen led to Li_2NH and some LiH. If the present samples contain small concentrations of LiH, its dissociation might yield free electrons and possibly protons. The present mobility seems much too high even for protons. Further, the formation enthalpy of LiH is given as 0.933 eV, essentially the same as that found here for c_0. Although the dissociation enthalpy of LiH within Li_3N would probably be different, this is still a suggestive coincidence.

Thus, we suggest that c_0 and D refer to electrons here, so that $D = D_n$. With this high a mobility at room temperature, if it is indeed present, Hall effect studies [27] could readily determine the mobility and the sign of the mobile carrier. Further, if the carriers are electrons there is no problem with the presence of a reaction resistance R_2 and reaction rate constants k_∞ and k_0. In addition, interaction of free electrons with the lattice by phonon scattering would lead to a decrease in mobility with increasing temperature, as indeed calculated from the present data. But it seems most unlikely that such a mechanism could yield the strong exponential dependence over the full temperature range we have inferred from R_1 and C_2 fitting. If the electrons move, on the other hand, between LiH molecules, or possibly even between neutral clumps of Li, one might expect that there would be fewer such entities the higher the temperature, and thus they would be farther and farther apart. Since their concentration would depend exponentially on temperature, one might expect that

the effective electron mobility would also show exponential dependence. Although these are highly tentative explanations, they do not seem impossible.

The above surprising $D(T)$ results depend entirely on the identification of $C_2 - C_1$ with the diffuse double layer capacitance C_{DL} and its conventional [11] association with the bulk charge density c_0 in $R_1 \equiv R_\infty$. But the need for a C_1 and the probable presence of an initial layer near the electrode of material different from Li_3N are not directly comprehended in the theoretical results employed for the above analysis. There is thus some chance that C_2 and R_2 should alternatively be considered together as applying to the interface layer alone and R_1 as applying to the Li_3N bulk. Then the c_0 obtained from C_2 and also present in R_2 would refer only to the interface layer material, not to the bulk Li_3N c_0 involved in R_1.

The above interpretation leads to $T/aR_2 = l^{-1}ec_I De/k$, where we have now written c_I for the bulk concentration in the interface layer. If we now use the T/aR_2 and c_0 (now interpreted as c_I) results of table 2, we find that $D = D_I \approx 7.182 \times 10^{-9}$ exp(0.453/kT). This expression leads to $D_I \approx$ 0.36 cm^2/s and 7.5×10^{-4} cm^2/s at 23.5°C and 182.3°C, respectively. Again it is D^{-1} which is thermally activated, but the associated ΔH is appreciably smaller than that found above. Although the D_I value at room temperature is appreciably smaller than the value of 2.75 cm^2/s calculated above, it still seems too large to be associated with ionic motion, and it thus appears necessary to assume that D_I refers to electronic motion. Unless the strong temperature dependence of C_2 can be explained in a plausible fashion without assuming that it is a double layer capacitance, it is difficult to avoid the present suggestion that conduction in the interface layer or perhaps in the entire sample L20 is dominantly electronic. One further possibility not included in eqs. (3) through (10) is that appreciable intrinsic (Frenkel) space charge layers are present near the electrodes, with their built-in potential differences strongly dependent on temperature. Under some circumstances, such dependence might lead to less derived c_0 temperature dependence and thus to more plausible diffusion coefficients.

It would be of interest to analyze admittance data for pure single crystal Li_3N without hydrogen by the same methods used herein to see if reasonable values of D_p for Li^+ could be obtained. We concede that the present results are quite surprising, being in conflict with the bulk of existing experimental evidence for pure ionic conduction in Li_3N. Von Alpen et al. [3] carried out both transference number measurements and dc polarization experiments on single crystal material and concluded that the observed conductivity was essentially entirely ionic with a partial electronic contribution of less than 10^{-12} Ω^{-1} cm^{-1} in the range 20–200°C. In that work, values of 1.2×10^{-3} Ω^{-1} cm^{-1} and 0.29 eV were measured for the conductivity at 300 K and activation enthalpy, respectively. Comparing those values with the results of Hooper et al. [4], we conclude that although the crystals used in the earlier work probably did contain some hydrogen, the concentration was probably lower than that for crystal L20 here. This difference may be significant. We believe the results presented here to be basically sound and hope that this demonstration of a detailed analysis of admittance data using complex least squares will prove instructive and useful.

Acknowledgement

We greatly appreciate the valuable comments and suggestions of Dr. J. Schoonman. This work was supported in part under U.S. National Science Foundation Grant No. DMR8005236.

References

[1] B.A. Boukamp and R.A. Huggins, Phys. Letters 58A (1976) 231.
[2] B.A. Boukamp and R.A. Huggins, Mat. Res. Bull. 13 (1978) 23.
[3] V. von Alpen, A. Rabenau and G.H. Talat, Appl. Phys. Letters 30 (1977) 621.
[4] A. Hooper, T. Lapp and S. Skaarup, Mat. Res. Bull. 14 (1979) 1617.
[5] J. Wahl, Solid State Commun. 29 (1979) 485.
[6] J.R. Macdonald and J.A. Garber, J. Electrochem. Soc. 124 (1977) 1022.
[7] J.R. Macdonald, J. Schoonman and A.P. Lehnen, J. Electroanal. Chem., to be published.
[8] J.R. Macdonald, 1980 Annual Report, 49th Conference on Electrical Insulation and Dielectric Phenomena, National Academy of Sciences (1980) pp. 3–49; Interface Effects in the Electrical Response of Non-metallic Conducting Solids and Liquids, Whitehead Memoria

Lecture, in 1980 Annual Report, 49th Conference on Electrical Insulation and Dielectric Phenomena, National Academy of Sciences, 27 October 1980, pp. 3–49. Reprinted with corrections in IEEE Transactions on Electrical Insulation, EI-15, 65–82, April (1981).
[9] J. Wahl and U. Holland, Solid State Commun. 27 (1978) 237.
[10] D.R. Franceschetti and J.R. Macdonald, J. Electroanal. Chem. 82 (1977) 277.
[11] J.R. Macdonald and D.R. Franceschetti, J. Chem. Phys. 68 (1978) 1614.
[12] D.R. Franceschetti and J.R. Macdonald, J. Electroanal. Chem. 101 (1979) 307.
[13] I.D. Raistrick, C. Ho and R.A. Huggins, J. Electrochem. Soc. 123 (1976) 1469.
[14] A.D. Franklin and K.F. Young, J. Electrochem. Soc. 124 (1977) 871.
[15] I.D. Raistrick, C. Ho, Y.-W. Hu and R.A. Huggins, J. Electroanal. Chem. 77 (1977) 319.
[16] A.K. Jonscher, Nature 267 (1977) 673;
K.L. Ngai, A.K. Jonscher and C.T. White, Nature 277 (1979) 185.
[17] J.R. Macdonald and M.K. Brachman, Rev. Mod. Phys. 28 (1956) 393.
[18] J.R. Macdonald and D.R. Powell, J. Res. Natl. Bur. Std. US 75A (1971) 441.
[19] J.R. Macdonald, J. Chem. Phys. 36 (1962) 345.
[20] J.R. Macdonald, J. Chem. Phys. 61 (1974) 3977.
[21] R.D. Armstrong and K. Taylor, J. Electroanal. Chem. 63 (1975) 9.
[22] K. Funke, in: Solid electrolytes, eds. P. Hagenmuller and W. van Gool (Academic Press, New York, 1978) p. 77.
[23] R.J. Grant, M.D. Ingram and A.R. West, J. Electroanal. Chem. 80 (1977) 239.
[24] D. Brinkmann, W. Freudenreich and J. Roos, Solid State Commun. 28 (1978) 233.
[25] W.F. Chu, H. Rickert and W. Weppner, in: Fast ion transport in solids, ed. W. van Gool (North-Holland, Amsterdam, 1973) p. 181.
[26] B.A. Boukamp and R.A. Huggins, Phys. Letters 72A (1979) 464.
[27] J.R. Macdonald and J.E. Robinson, Phys. Rev. 95 (1954) 44.